JCTC Journal of Chemical Theory and Computation

ARTICLE

pubs.acs.org/JCTC

Absolute Entropy and Energy of Carbon Dioxide Using the Two-Phase Thermodynamic Model

Shao-Nung Huang,[†] Tod A. Pascal,[‡,§] William A. Goddard, III,[‡,§] Prabal K. Maiti,[∥] and Shiang-Tai Lin*[,†]

[†]Department of Chemical Engineering, National Taiwan University, Taipei 10617, Taiwan

[‡]Materials and Process Simulation Center, Beckman Institute, California Institute of Technology, Pasadena, California 91125, United States

[§]Graduate School of EEWS (WCU), Korea Advanced Institute of Science and Technology, Daejeon 305-701, Republic of Korea

[∥]Centre for Condensed Matter Theory, Department of Physics, Indian Institute of Science, Bangalore 560012, India

ABSTRACT: The two-phase thermodynamic (2PT) model is used to determine the absolute entropy and energy of carbon dioxide over a wide range of conditions from molecular dynamics trajectories. The 2PT method determines the thermodynamic properties by applying the proper statistical mechanical partition function to the normal modes of a fluid. The vibrational density of state (DoS), obtained from the Fourier transform of the velocity autocorrelation function, converges quickly, allowing the free energy, entropy, and other thermodynamic properties to be determined from short 20-ps MD trajectories. The anharmonic effects in the vibrations are accounted for by the broadening of the normal modes into bands from sampling the velocities over the trajectory. The low frequency diffusive modes, which lead to finite DoS at zero frequency, are accounted for by considering the DoS as a superposition of gas-phase and solid-phase components (two phases). The analytical decomposition of the DoS allows for an evaluation of properties contributed by different types of molecular motions. We show that this 2PT analysis leads to accurate predictions of entropy and energy of CO_2 over a wide range of conditions (from the triple point to the critical point of both the vapor and the liquid phases along the saturation line). This allows the equation of state of CO_2 to be determined, which is limited only by the accuracy of the force field. We also validated that the 2PT entropy agrees with that determined from thermodynamic integration, but 2PT requires only a fraction of the time. A complication for CO_2 is that its equilibrium configuration is linear, which would have only two rotational modes, but during the dynamics it is never exactly linear, so that there is a third mode from rotational about the axis. In this work, we show how to treat such linear molecules in the 2PT framework.

1. INTRODUCTION

Carbon dioxide (CO_2) is an important chemical in the biosphere. It is the source of carbon for photosynthetic generation development of plants and the product of respiration in animals. Industrial societies produce a great deal of CO_2 from combustion and other chemical processes, and it is a popular solvent for supercritical extraction. Above its critical pressure (72.9 atm) and temperature (304.2 K), carbon dioxide behaves as a supercritical fluid: it has the diffusion constant of a gas, while maintaining the density of a liquid. This behavior facilitates the use of supercritical CO_2 ($scCO_2$) in a wide range of industrial processes, from chemical extraction[1,2] to petroleum recovery.[3,4] Recent studies have focused on utilizing liquid and $scCO_2$ as a cost-effective "green" solvent[5] for chemical reactions, owing to low toxicity, high availability, and catalytic ability.[6,7] More recently there is great concern that CO_2 is responsible for anthropomorphic climate change, responsible for global warming, which is stimulating many efforts to capture and sequester CO_2.[8−10] The knowledge of thermodynamic properties of CO_2 under various conditions and with various additional components is important for studying such CO_2 related problems.

Computer simulations (molecular dynamics, Monte Carlo, quantum mechanics) are powerful tools used to estimate physical properties of CO_2. Of particular interest are the vapor−liquid coexistence curve,[11−16] supercritical behavior (thermodynamics,[15,16] transport properties,[11,16−18] structural properties,[11,15,16,19,20] other properties[20−22]), and properties of solid CO_2.[23] The CO_2 molecule is unique due to its linear structure, zero dipole moment, and large quadruple moment.[24] However, in a dynamics collection of CO_2 molecules, it is essentially always nonlinear.[15,19−21] This change in character contributes to the special properties of CO_2, particularly in the supercritical state, and challenges the prediction of its properties using molecular simulations. A thermodynamic property of particular interest is the absolute entropy. Recently, some theory and methods have been developed to estimate the absolute entropy and/or solvation free energy. However, most focus on water,[25−27] aqueous solutions,[28−30] or glass-like systems.[25,31] There is no report on the performance of such methods for linear molecules such as CO_2.

The two-phase thermodynamic (2PT) method is an efficient way to estimate thermodynamic properties (energy, entropy, and heat capacity) of a system. This method has been shown to provide accurate properties using a short (about 20 ps) MD trajectory for systems such as Lennard-Jones fluids,[32] liquid−vapor water along the coexistence curve,[33] and many common organic liquids under standard conditions.[34] The 2PT

Received: March 27, 2011
Published: May 16, 2011

method has also been successfully used in calculating the entropy of water in different regions such as the dendrimer,[35] lipid bilayer,[36] and carbon nanotube.[37] The method is also reasonably accurate in describing the entropic penalty of DNA while binding to dendrimer[38] as well as describing the role of counterion release entropy in macromolecular complexation.[39,40] In this work, we present the use of 2PT in the property determination of CO_2. We validate the 2PT determined entropy by comparing it to those determined from thermodynamic integration (TI).

2. THEORY

2.1. Density of State Function and Its Decomposition. The density of state function, $S(\upsilon)$, which is defined as the sum of mass-weighed atomic spectral densities, can be obtained from the Fourier transform of velocity autocorrelation function (VACF),[32,33] or equivalently the velocity spectrum[41]

$$S(\upsilon) = \frac{1}{k_B T}\sum_{l=1}^{N}\sum_{k=1}^{3}\lim_{\tau\to\infty}\frac{m_l}{\tau}\left|\int_{-\tau}^{\tau} v_l^k(t)\, e^{-i2\pi\upsilon t}\, dt\right|^2 \quad (1)$$

where N is the total number of atoms in the system, m_l is the mass of atom l, and v_l^k is the velocity of atom l in the k direction (k = 1−3 represents x, y, and z directions, respectively). The function $S(\upsilon)$ is the distribution of normal modes of the system, i.e., $S(\upsilon)$ $d\upsilon$ represents the number of normal modes with frequencies from υ to $\upsilon + d\upsilon$. The integration $S(\upsilon)$ gives the total degrees of freedom (DF) $3N$; i.e.

$$\int_0^\infty S(\upsilon)\, d\upsilon = 3N \quad (2)$$

(Note that in MD simulations the translational degrees of freedoms are removed for the conservation of linear momentum; therefore, the integration gives $3N - 3$ instead.) For a pure monatomic system, the zero-frequency density of state is associated with the diffusion coefficient of particles[32,33]

$$D = \frac{k_B T}{12mN} S(0) \quad (3)$$

where T is the temperature and k_B is the Boltzmann constant.

For systems of polyatomic molecules, Lin et al.[33] suggested that the $S(\upsilon)$ be decomposed into three components: translation (trn), rotation (rot), and intramolecular vibration motions (imv):

$$S(\upsilon) = S_{trn}(\upsilon) + S_{rot}(\upsilon) + S_{imv}(\upsilon) \quad (4)$$

where the translation component is obtained from the center of mass velocity of the molecules

$$S_{trn}(\upsilon) = \frac{1}{k_B T}\sum_{j=1}^{M}\sum_{k=1}^{3}\lim_{\tau\to\infty}\frac{m_j}{\tau}\left|\int_{-\tau}^{\tau} v_j^{*k}(t)\, e^{-i2\pi\upsilon t}\, dt\right|^2 \quad (5)$$

where M is the total number of molecules in the system, m_j is the mass of molecule j, and v_j^{*k} is the center of mass velocity of molecule j in the k direction. The rotational density of state function is determined by using the following equations:

$$S_{rot}(\upsilon) = \frac{1}{k_B T}\sum_{j=1}^{M}\sum_{k=1}^{3(2)}\lim_{\tau\to\infty}\frac{I_j^k}{\tau}\left|\int_{-\tau}^{\tau} \omega_j^k(t)\, e^{-i2\pi\upsilon t}\, dt\right|^2 \quad (6)$$

where ω_j^k and I_j^k are the angular velocity and moment of inertia of molecule j along the kth principal axis, respectively. For nonlinear molecules (e.g., water), there are three nonzero principle moments of inertia. For linear molecules (e.g., nitrogen and carbon dioxide), there are only two nonzero principle moments of inertia, and the value of k runs from 1 to 2.

The intramolecular velocity can be determined by subtracting the center of mass translation and rotation velocities

$$\vec{v}_l^{imv} = \vec{v}_l - \vec{v}_j^{*} - \vec{\omega}_j \times \vec{r}_{lj} \quad (7)$$

where $\vec{r}_{lj}$ is the position vector of atom l from the center of mass of molecule j. Using the intramolecular velocity in eq 1 leads to the corresponding component of the density of state function.

2.2. Thermodynamic Properties from Two-Phase Thermodynamic (2PT) Model. The thermodynamic properties (absolute entropy, energy, and heat capacity) are determined from the sum of translation, rotation, and intramolecular vibration contributions[33]

$$E = E_0 + E_{trn} + E_{rot} + E_{imv} \quad (8)$$

$$S = S_{trn} + S_{rot} + S_{imv} \quad (9)$$

$$Cv = \frac{dE_0}{dT} + Cv_{trn} + Cv_{rot} + Cv_{imv} \quad (10)$$

where E_0 is the reference energy.[33] For a system containing only harmonic motions (e.g., crystals), its thermodynamic properties can be calculated exactly from the density of state $S(\upsilon)$ based on statistical mechanics for harmonic oscillators. For fluids, such a harmonic approximation is no longer valid because of the significant anharmonic nature of the low frequency modes. In particular, the zero-frequency (diffusive) modes would lead to diverged properties. In the two-phase thermodynamic (2PT) model, the anharmonic effects are treated by dividing the density of state distribution into solid-like and gas-like components, i.e.

$$S_m(\upsilon) = S_m^s(\upsilon) + S_m^g(\upsilon) \quad (11)$$

where the subscript m denotes the translation (trn) or rotation (rot) component. The gas component is determined accordingly based on the DoS at zero frequency and the fluidicity factor f_m

$$S_m^g(\upsilon) = \frac{S_m(0)}{1 + \left[\frac{\pi\upsilon S_m(0)}{6 f_m M}\right]^2} \quad (12)$$

and the fluidicity factor f_m is determined from the dimensionless diffusivity constant Δ_m as

$$2\Delta_m^{-9/2} f_m^{15/2} - 6\Delta_m^{-3} f_m^5 - \Delta_m^{-3/2} f_m^{7/2} + 6\Delta_m^{-3/2} f_m^{5/2} + 2f_m - 2 = 0 \quad (13)$$

with

$$\Delta_m(T, V, M, m, S_m(0)) = \frac{2S_m(0)}{9M}\left(\frac{\pi k_B T}{m}\right)^{1/2}\left(\frac{N}{V}\right)^{1/3}\left(\frac{6}{\pi}\right)^{2/3} \quad (14)$$

Equation 12 ensures that all of the diffusive modes are included in the gas-like component, i.e., $S(0) = S^g(0)$. The integration of eq 12 over frequency gives the degrees of freedom of the gas-like component, $3Mf_m$. Once the gas-like component is determined, the solid-like component can be obtained from the difference between the total DoS and the gas-like DoS from eq 11.

Once the DoS are available, the thermodynamic properties can be expressed as the integral of the density of state function weighed by the corresponding weighting functions for the j component of different motions $W_{i,m}^{j}(\upsilon)$ (i = E, S, or Cv; j = s or g; m = trn, rot, or imv)

$$E_m = \beta^{-1}\left[\int_0^\infty d\upsilon\, S_m^s(\upsilon)\, W_{E,m}^s(\upsilon) + \int_0^\infty d\upsilon\, S_m^g(\upsilon)\, W_{E,m}^g(\upsilon)\right] \quad (15)$$

$$S_m = k_B\left[\int_0^\infty d\upsilon\, S_m^s(\upsilon)\, W_{S,m}^s(\upsilon) + \int_0^\infty d\upsilon\, S_m^g(\upsilon)\, W_{S,m}^g(\upsilon)\right] \quad (16)$$

$$Cv_m = k_B\left[\int_0^\infty d\upsilon\, S_m^s(\upsilon)\, W_{Cv,m}^s(\upsilon) + \int_0^\infty d\upsilon\, S_m^g(\upsilon)\, W_{Cv,m}^g(\upsilon)\right] \quad (17)$$

where $\beta = (k_B T)^{-1}$. The weighing functions are

$$W_E^s(\upsilon) = \frac{\beta h\upsilon}{2} + \frac{\beta h\upsilon}{\exp(\beta h\upsilon) - 1} \quad (18)$$

$$W_S^s(\upsilon) = \frac{\beta h\upsilon}{\exp(\beta h\upsilon) - 1} - \ln[1 - \exp(-\beta h\upsilon)] \quad (19)$$

$$W_{Cv}^s(\upsilon) = \frac{(\beta h\upsilon)^2 \exp(\beta h\upsilon)}{[\exp(\beta h\upsilon) - 1]^2} \quad (20)$$

$$W_{E,\mathrm{trn}}^g(\upsilon) = W_{E,\mathrm{rot}}^g(\upsilon) = W_{Cv,\mathrm{trn}}^g(\upsilon) = W_{Cv,\mathrm{rot}}^g(\upsilon) = 0.5 \quad (21)$$

$$W_{S,\mathrm{trn}}^g(\upsilon) = \frac{1}{3}\frac{S^{\mathrm{HS}}}{k_B} \quad (22)$$

$$W_{S,\mathrm{rot}}^g(\upsilon) = \frac{1}{3}\frac{S^{\mathrm{R}}}{k_B} \quad (23)$$

where S^{HS} and S^{R} are the hard-sphere entropy and rotational entropy of molecules (rigid rotor) at the ideal gas state, respectively:

$$\frac{S^{\mathrm{HS}}}{k} = \frac{5}{2} + \ln\left[\left(\frac{2\pi mkT}{h^2}\right)^{3/2}\frac{V}{f_{\mathrm{trn}}N}z(y)\right] + \frac{y(3y-4)}{(1-y)^2} \quad (24)$$

$$\frac{S^{\mathrm{R}}}{k} = 1 + \ln\left[\frac{T}{\sigma\Theta_r}\right] \quad (25)$$

where $y = {f_{\mathrm{trn}}}^{5/2}/{\Delta_{\mathrm{rn}}}^{3/2}$ and $z(y)$ is the compressibility factor of hard sphere gases from the Carnahan−Starling equation of state,[42] $\Theta_r = h^2/(8\pi^2 I_r k)$ is the rotation temperature, and σ is the symmetry number. It is noteworthy that the 2PT method includes quantum correction by applying the harmonic oscillator (HO) approximation for the canonical partition function Q, which is included in the weighting function of the solid-like components.[32,33] The reference energy is obtained by comparing the MD potential energy to the 2PT energy based on classical harmonic oscillators[33]

Table 1. FEPM2 Force Field Parameters for CO_2[a]

element	ε/k_b (K)	σ (Å)	q (e)
O	80.507	3.033	−0.3256
C	28.129	2.757	0.6512
l_0 (Å)	1.149	K_b (kcal/mol/Å^2)[b]	1283.38
θ_0 (deg)	180	K_θ (kcal/mol/rad^2)[b]	56.53

[a] ε and σ are the Lennard-Jones parameters in the LJ-12−6 potential $E^{\mathrm{vdw}}(r) = 4\varepsilon[(\sigma/r)^{12} - (\sigma/r)^6]$. q is the atomic charge for calculation of electrostatic energy. The valence energy for CO_2 is $E^{\mathrm{valence}} = E^{\mathrm{bond}} + E^{\mathrm{angle}} = K_b(l - l_0)^2 + K_\theta(\theta - \theta_0)^2$, where l_0 is the equilibrium C═O bond length, θ_0 is the equilibrium OCO angle, and K_b and K_θ are the stretching and bending force constants, respectively. [b] The value of K_b and K_θ are taken from refs 17 and 21, respectively; all other parameters are from ref 14.

$$E_0 = E_{\mathrm{MD}} - \beta^{-1}3N(1 - 0.5f_{\mathrm{trn}} - 0.5f_{\mathrm{rot}}) \quad (26)$$

where E_{MD} is the total energy of the system from the same MD simulation.

3. COMPUTATIONAL DETAILS

The open-source LAMMPS[43] package is used for the molecular dynamic simulations. The absolute entropy and energy of CO_2 fluid are determined along the experimental vapor−liquid equilibrium (VLE) conditions and compared to the experimental data. The experimental VLE data are taken from the steam table.[44] Three-dimensional periodic models of 256 molecules at desired densities are created for the subsequent molecular dynamic simulations.

The flexible version of the EPM2 force field (FEPM2; original EPM2[14] with the stretching force constant by Nieto-Draghi et al.[17] and bending force constant by Anderson et al.;[21] parameters are listed in Table 1) is used to describe the interactions in the system. The two force constants were fitted to the vibration frequencies of symmetric stretching and angle bending, respectively. We compare the vibration frequencies of CO_2 with the experimental data[45] in Table 2.

Energy minimization is performed on the initial structure. A long 4 ns MD simulation at constant volume and temperature (NVT) follows to equilibrate the system. To facilitate thermal equilibration between different types of motion (translation, rotation, and vibration), the three temperatures associated with each motion type are rescaled to the system temperature by rescaling the velocities of the corresponding motions at a time interval of 1 ps. We will show that such a velocity rescaling is critical for obtaining thermal equilibration in CO_2. The system is further equilibrated using an additional 1 ns NVT simulation without such a velocity rescaling. An additional 20 ps simulation for sampling is performed with the trajectory saved at every 4 fs for the 2PT property analysis. We have examined and confirmed that thermodynamic properties of CO_2 from 2PT analysis converge within 20 ps, which is consistent with previous findings.[33,34]

The integration time step is set to 1 fs. The time constants for the Nose-Hoover thermostat[46] and velocity rescaling are set to 0.1 and 1 ps, respectively. The long-range electrostatic interaction is estimated by the particle−particle particle-mesh Ewald method[47] (pppm) with an accuracy of 4.18×10^{-5} kJ/mol. The cutoff radii for the pppm and van der Waals interaction are 8.5 Å

Table 2. Comparison of Intramolecular Vibration Frequencies of CO_2 from the Experiment and MD Simulations

vibration modes	NIST data[45] (gas phase)	this work (220 K, sat'd liquid)	this work (220 K, sat'd vapor)
symmetric stretching	1285.40 (Raman)	1326	1324
	1388.15 (Raman)	1418	1416
angle bending	667.38 (IR)	679	681
asymmetric stretching	2349.16 (IR)	2659	2658

and 9.5 Å for liquid-phase simulations. For vapor phase simulations, we use a cutoff radius of 17.0 Å for more efficient pppm calculations.[48]

To validate the accuracy of the entropy from the 2PT model, we compared it to the results from thermodynamic integration (TI) for CO_2 from 220 K to 600 K. Since TI leads only to an entropy difference between two state points, whereas 2PT leads to absolute entropies, we take the difference between the absolute 2PT entropies.

The way to determine the density-of-state function for translation, rotation, and intramolecular vibration has been detailed elsewhere.[33] Briefly, the center of mass velocity ($\vec{v}^*$), the angular moment ($\vec{L}$), and the inertia tensor ($\bar{\bar{I}}$) are determined for every molecule at each time instant. The principle moments of inertia (I_1, I_2, and I_3) and the principal axis ($\vec{p}_1$, $\vec{p}_2$, and $\vec{p}_3$) are then obtained by solving the eigenvalue and eigenvector of the inertia tensor. The angular velocity along the principal axis can be calculated by $\vec{\omega}_i = (\vec{L} \cdot \vec{p}_i / I_i)\vec{p}_i$. The velocity component due to intramolecular vibration ($\vec{v}^{\text{imv}}$) can then be determined from eq 7. These velocity components allow for the determination of the corresponding DoS using eqs 5 (trn), 6 (rot), and 1 (vib). It should be noted that while carbon dioxide is regarded as a linear molecule, it is almost never linear in the molecular dynamic simulations. For example, Saharay and Balasubramanian[19] reported the average value of the angle OCO to be 174.2° on the basis of the Car−Parrinello molecular dynamic simulations. In practice, CO_2 has two large principle moments of inertia (I_1 = I_2 = 43.4 g/mol Å^2) and a third one that fluctuates around zero (I_3 = ~0.01 g/mol Å^2). Therefore, we have set I_3 and ω_3 to zero and therefore attribute such motions as part of the intramolecular vibration.

4. RESULTS AND DISCUSSION

4.1. The Density of State of Carbon Dioxide. Figure 1 shows the DoS spectrum of liquid FEPM2 CO_2 at T = 220 K. The decomposition of $S(\upsilon)$ to translation, rotation, and internal vibration is also presented. The broad band between 0 and 200 cm^{-1} represents the modes corresponding to librations. Intramolecular vibrations are observed in the higher frequency region: angle bending at 679 cm^{-1}, symmetric stretching at 1326 and 1418 cm^{-1}, and asymmetric stretching at 2660 cm^{-1} (also listed in Table 2). The splitting peaks of symmetric stretching is a result of the Fermi resonance.[49,50] Both the translation and rotation motions contribute to the zero-frequency density of state function $S(0)$, indicating translational and rotational diffusion in the system.

Figure 1b and c illustrate the decomposition of translation DoS, $S_{\text{trn}}(\upsilon)$, and rotational DoS, $S_{\text{rot}}(\upsilon)$, to gas-like and solid-like contributions. It can be seen that the 2PT method nicely

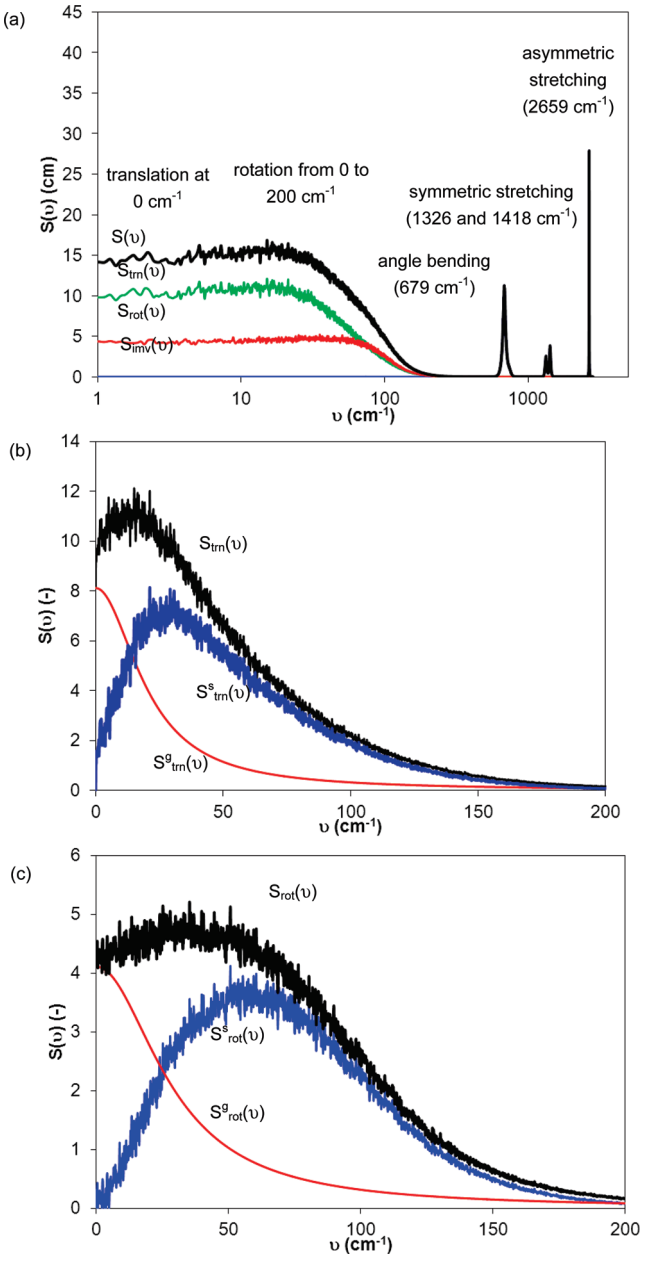

Figure 1. (a) Density of state spectrum of liquid CO_2 at 220 K and 1.1663 g/cm^3 from 200-ps sampling. (b) Translation density of state and its components. (c) Rotation density of state and its components. This illustrates the various DoS components used in the 2PT analysis.

separates the DoS to an exponentially decaying gas-like component and a solid-like component with its intensity approaching zero at zero frequency.

4.2. Thermodynamic Properties of CO_2. To illustrate the applicability of 2PT over a wide range of state conditions, the entropy and energy of CO_2 are determined at temperatures and densities[44] along the vapor−liquid coexistence curve. Table 3 summarizes the calculation results of the temperatures of the molecular motions, internal energy, and absolute entropy and compares the 2PT calculations with the experimental data.[44] The fluidicity factors increase from 0.36 (translation) and 0.25 (rotation) for the liquid at 220 K to 0.70 and 0.48 at the critical point (304 K), and to 0.89 and 0.81 for the vapor at 220 K. The

Table 3. Comparison between 2PT Properties of FEPM2 CO_2 and the Experimental Data[44a]

state of aggregation	d	T	S_{2PT}	S_{exp}	E_{2PT}	E_{md}	E_{exp}	f_{trn}	f_{rot}
saturated liquid	1.1663	220	111.82	118.12	18.91	17.71	17.25	0.36	0.25
	1.1292	230	116.56	121.59	19.16	18.85	18.06	0.40	0.26
	1.0896	240	119.38	125.07	19.90	20.04	18.88	0.42	0.28
	1.0467	250	123.68	128.64	21.04	21.18	19.74	0.44	0.29
	1.0000	260	127.50	132.24	21.30	22.39	20.65	0.47	0.31
	0.9470	270	131.35	135.94	22.34	23.65	21.61	0.51	0.33
	0.8850	280	136.79	139.77	22.91	24.88	22.64	0.53	0.35
	0.8058	290	141.66	143.95	24.76	26.27	23.81	0.57	0.39
	0.6803	300	147.53	149.32	26.50	28.18	25.33	0.63	0.43
critical point	0.4662	304	156.09	156.58	27.52	30.36	27.32	0.70	0.48
saturated vapor	0.2703	300	163.86	164.68	29.76	31.99	29.28	0.78	0.58
	0.1724	290	169.50	169.61	30.03	32.53	30.19	0.82	0.64
	0.1220	280	171.63	172.73	30.12	32.65	30.59	0.85	0.69
	0.0885	270	175.25	175.20	29.93	32.36	30.78	0.87	0.71
	0.0645	260	177.07	177.44	30.57	32.26	30.86	0.88	0.73
	0.0467	250	179.85	179.51	30.78	31.77	30.87	0.89	0.77
	0.0333	240	182.56	181.67	30.81	31.45	30.82	0.90	0.79
	0.0234	230	184.35	183.87	30.66	31.06	30.74	0.89	0.80
	0.0160	220	186.71	186.24	30.62	30.62	30.62	0.89	0.81

[a] Reference state of energy: saturated vapor at 220 K. Units: T in K, E in kJ/mol, S in J/mol/K, and d in g/cm^3.

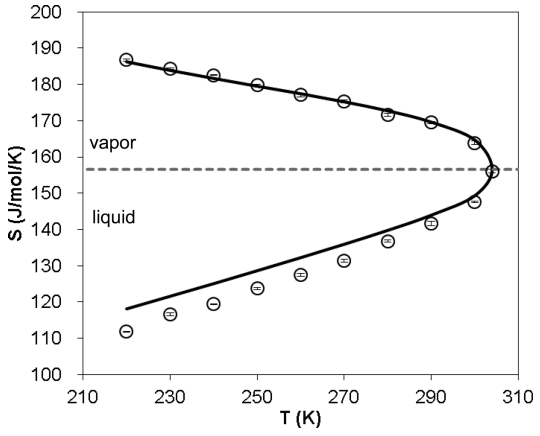

Figure 2. The absolute entropy of CO_2 along the vapor−liquid coexistence curve (for CO_2, T_{tp} = 216.6 K and T_c = 304.2 K) calculated by the 2PT model (open circle) from 20-ps MD trajectories. The results are compared with the experimental data[44] (black solid line). The gray dashed line indicates the entropy at the critical state. This shows that 2PT can provide a reliable entropy of CO_2 vapor and liquid over a wide range of conditions.

increase of the fluidicity factor implies the increasing gas-like nature of the fluid as its density decreases along the coexistence curve. Figures 2 and 3 illustrate the absolute entropy S(2PT) and its components (S_{trn}, S_{rot}, and S_{imv}) along the vapor−liquid coexistence curve. The 2PT entropies are in excellent agreement with experimental results in the vapor phase. The discrepancy between 2PT entropy and experimental results increases with increasing density, with the largest error observed for the saturated liquid at 220 K (5.3%). Furthermore, the

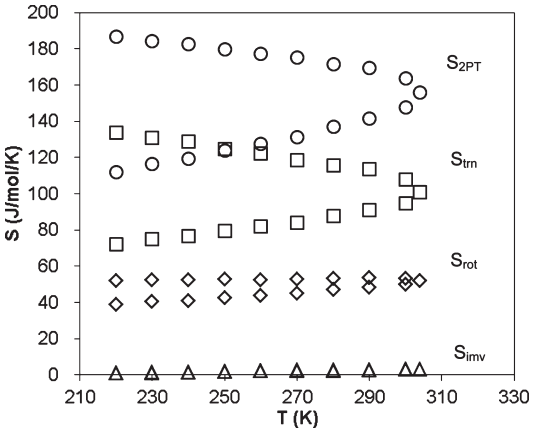

Figure 3. The absolute entropy (S_{2PT}) its components (S_{trn}, S_{rot}, S_{imv}) of CO_2 along the vapor−liquid coexistence curve. This shows that the entropy of CO_2 is dominated by contributions from translation and rotational motions.

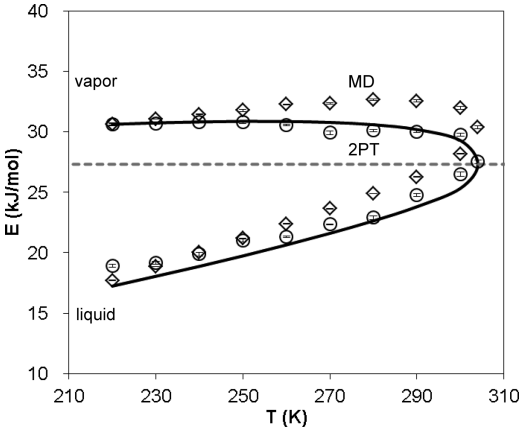

Figure 4. The internal energy of CO_2 along the vapor−liquid coexistence curve calculated by the 2PT model (open circle) from 20-ps MD trajectories. The results are compared with classical energy from MD simulations (open diamond) and the experimental data[44] (black solid line). The gray dashed line indicates the energy at the critical state. This shows that while MD energy difference between the vapor and liquid phases (energy of vaporization) may be consistent with experimental data, the value in each individual phase is incorrect. The 2PT energies are in better agreement with the experimental data for both phases.

intramolecular vibration entropy S_{imv} is negligible compared to the other two components (S_{trn} and S_{rot}) in all cases (see Figure 3). The change of entropy along the coexistence curve is dominated by S_{trn}, meaning that the change of density and temperature affects the translational motion most. S_{rot} is about constant in the vapor phase, whereas it increases in the liquid phase with increasing temperature and decreasing density. That is, under high-density conditions, the rotational motion of CO_2 molecules is hindered by the surrounding molecules, while the molecular rotation hindrance is insignificant at low density because of the weaker intermolecular interaction.

Figure 4 shows the energy along the vapor−liquid coexistence curve. It is interesting to note that the total energy E_{md} from MD (sum of kinetic and potential energies, shown in open diamonds) is overestimated in both phases, especially near the critical point, when compared to the experimental data (solid curve). This

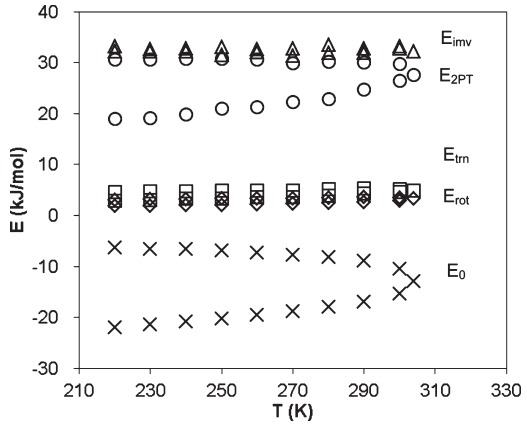

Figure 5. The internal energy (E_{2PT}) and its components (E_0, E_{trn}, E_{rot}, E_{imv}) of CO_2 along the vapor−liquid coexistence curve. This shows that the total energy E_{2PT} is dominated by the reference energy E_0.

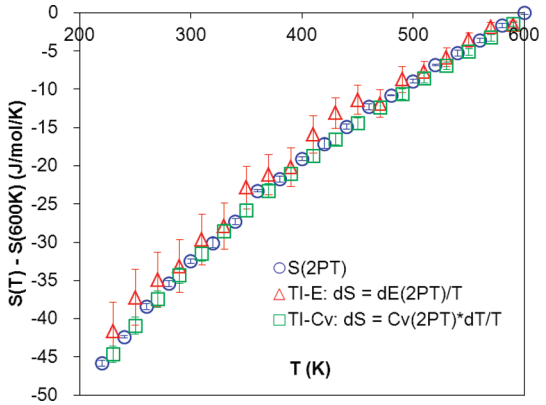

Figure 6. The relative entropy of CO_2 (d = 1.1663 g/cm^3, the saturated liquid density at 220 K) from T = 600 to 220 K using the 2PT method and thermodynamic integration calculations. This shows that the 2PT entropies are consistent with those determined from TI.

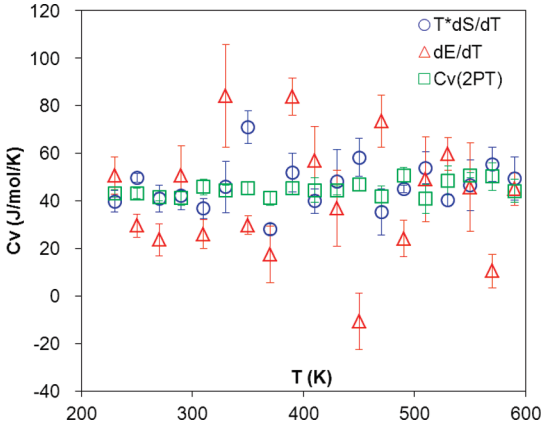

Figure 7. The constant volume heat capacity of liquid CO_2 (d = 1.1663 g/cm^3, the saturated liquid density at 220 K) from T = 600 to 220 K. Triangle, calculated from $Cv = dE_{2PT}/dT$; square, heat capacity directly from 2PT method (eq 17); circle, from TdS_{2PT}/dT. This shows that the direct calculation of the specific heat from the 2PT DoS is much more accurate than deriving it from the changes in the calculated properties of other variables.

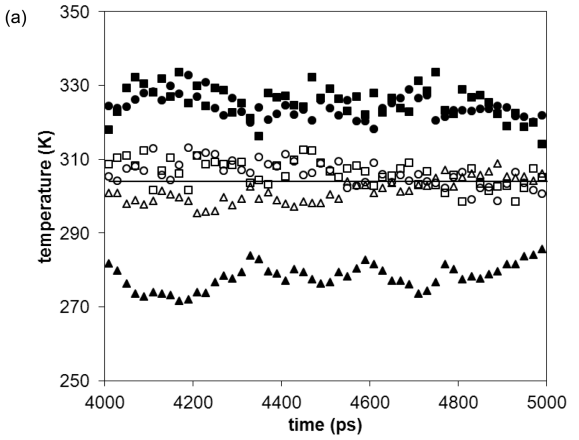

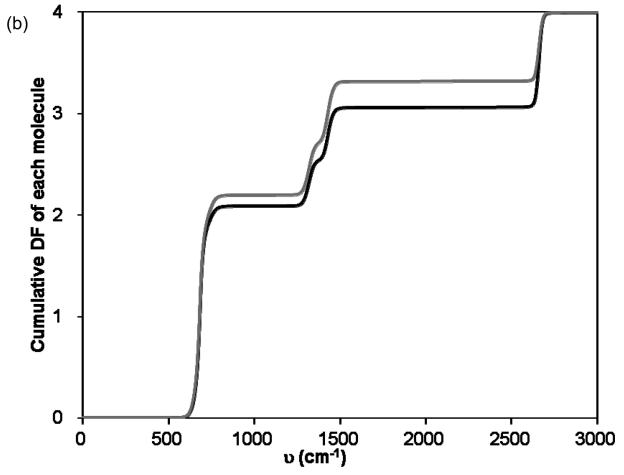

Figure 8. (a) The temperature components (circles for translation T_{trn}, squares for rotation T_{rot}, and triangles for intramolecular vibration T_{imv}) from the simulations of CO_2 at the critical point. The closed symbols indicate temperatures in the 5th ns from a regular NVT simulation. The open symbols represent results if the first 4 ns are subjected to velocity rescaling. (b) Cumulative vibration degrees of freedom of the intramolecular vibrations from simulations with (solid line) and without (gray line) velocity rescaling. This shows that velocity rescaling provides effective means for energy exchange between different modes of motions in CO_2.

indicates that, while the heat of vaporization obtained from E_{md} may be consistent with experimental data over a wide range of temperatures, the (dynamic and thermodynamic) properties may be in error in both the vapor and liquid phases. In contrast, the 2PT energies, which take the quantum correction into consideration, are in good agreement with the experiment. The components of the total energy E_{2PT} are illustrated in Figure 5. In both phases, E_{trn} and E_{rot} slightly increase with the increasing temperature, whereas E_{imv} is nearly constant. The change of the reference energy (E_0) dominates the temperature and density dependence of E_{2PT}. It is noteworthy that the fluctuations observed in E_{2PT} are a result of the fluctuation in E_{imv}, which is affected by the energy equilibration between different vibrational modes.

4.3. Comparison of Entropy from 2PT and Thermodynamic Integration. Here, we validate the entropy change of CO_2 between two thermodynamic states from 2PT with that from thermodynamic integration (TI). The entropy change by

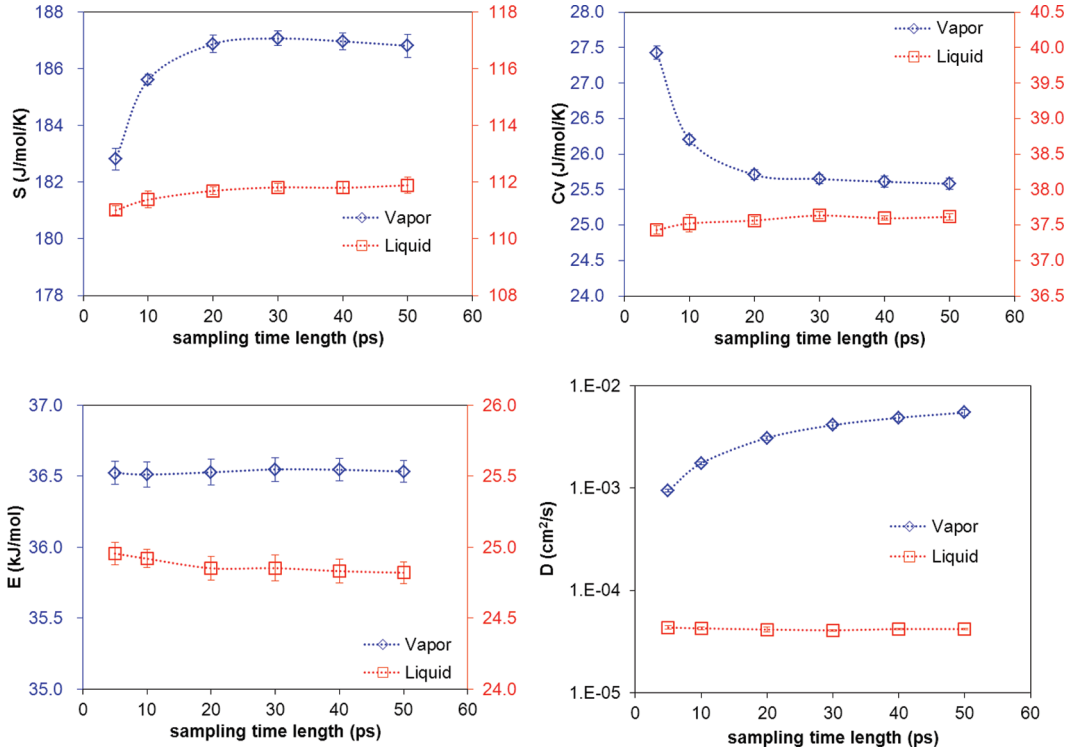

Figure 9. The 2PT thermodynamic (S, E, and Cv) and transport (diffusivity D) properties evaluated using different lengths of trajectories for saturated vapor (open diamonds) and liquid (open squares) CO_2 at 220 K. The error bars (of all the figures presented in this paper) indicate the standard deviations from four samplings. This shows that the 2PT thermodynamic properties converge within 20 ps.

heating a fluid from T_1 to T_2 under constant volume can be obtained from the temperature integration of the energy (referred to as TI-E) or constant volume heat capacity (TI-Cv) as follows:

$$S(T_2,d) - S(T_1,d) = \int_{T_1}^{T_2} \frac{dE_{2PT}(T',d)}{T'dT'}\,dT' \qquad (27)$$

$$S(T_2,d) - S(T_1,d) = \int_{T_1}^{T_2} \frac{C_{V,2PT}(T',d)}{T'}\,dT' \qquad (28)$$

where d is the density of the system. Figure 6 shows the calculated entropy change of CO_2 from a saturated liquid at T_1 = 220 K (d = 1.17 g/cm^3) to a higher temperature (up to 600 K) under constant density. Twenty sets of simulations were performed at a temperature interval of 20 K between 220 and 600 K. The parameters and settings for the simulations are the same as the previous cases. Note that temperature 600 K is well above the critical temperature of CO_2 (at 304.2 K), so the fluid behaves like a system of hard spheres. The integrations in eq 27 and 28 are calculated numerically on the basis of the midpoint trapezoidal rule. It can be seen that the entropy changes calculated from 2PT (open sphere) and TI (open triangle for TI-E and open square for TI-Cv) are identical within statistical uncertainty.

It should be noted that the relatively large standard deviation seen in TI-E is a result of the energy fluctuations, mainly due to intramolecular vibrations. Figure 7 compares the heat capacity from the numerical derivative of energy (Cv = $(\partial E(2PT))/(\partial T)|_d$), entropy ($Cv$ = $(T\partial S(2PT))/(\partial T)|_d$), and the value directly obtained from eq 17. The 2PT heat capacity (open squares) is nearly constant with the increasing of temperature, whereas the temperature derivative of either the energy (open triangles) or the entropy (open spheres) shows significant fluctuations. The fluctuation in the DoS distribution (especially in the high frequency region, i.e., internal vibrations) causes about 0.5−1 kJ/mol fluctuations in energy, resulting in 10^1∼10^2 J/mol K fluctuations in heat capacity from the numerical derivative of E. While such fluctuations may be reduced by longer simulations, the 2PT is capable of providing converged properties (e.g., Cv) without the use of exhaustive samplings.

4.4. Thermal Equilibration in CO_2 Simulations. We notice that there is a weak coupling of internal vibrational and libration modes with collisions for molecules like CO_2 with no net dipole. As a result, there is a poor thermal equilibration between different types of motions (translation, rotation, and vibration) in the system. Figure 8a illustrates the temperatures determined from the corresponding kinetic energies of a simulation at the critical point (304.2 K and 0.47 g/cm^3). The temperatures are calculated from the last 1 ns of a 5 ns NVT simulation. It is seen that the translation and rotational temperatures (closed circles and squares) fluctuate around 325 K, while the intramolecular vibration temperature (closed triangles) fluctuates around 275 K over a time period of 1 ns. The slow convergence of these temperatures indicates a poor energy exchange between different types of motions in CO_2. Also shown in Figure 8a are the temperature components (open symbols) from a simulation that has been subjected to velocity rescaling (as described in the Computational Details) in the first 4 ns of simulation. It is seen that the velocity rescaling effectively equilibrates the kinetic energies of different types of motions. The system remains in good thermal equilibration even without the velocity rescaling in the fifth ns. The velocity rescaling is also important for obtaining

the correct distribution of the degrees of freedom for the internal vibrations (two angle bending, one symmetric, and one asymmetric stretching). Figure 8b shows that the DFs of angle bending and symmetric stretching are overestimated (by 0.2 and 0.1, respectively) if the temperatures associated with different motions are not fully equilibrated (the gray line). When a good equilibration is reached, a proper DF distribution is obtained (black line). The distribution of DF has a significant impact on the energy associated with vibrations (especially the zero point energy). We note that if the DF of angle bending of CO_2 is 3% higher than the expected value (2), E_{imv} will be about 0.5 kJ/mol too low.

4.5. Convergence of Thermodynamic Properties. Figure 9 shows the thermodynamic and transport properties of saturated vapor and liquid CO_2 at 220 K evaluated using different lengths of MD trajectory. It can be seen that thermodynamic properties (*E*, *S*, and *Cv*) are converged within 20 ps for both phases, even though the diffusivity is not fully converged. Similar results have been reported for other organic solvents.[34] While the gas−solid decomposition in 2PT relies on the value of diffusivity, there seems to be a good balance between the calculated properties in from the solid and gas components such that the total property is not sensitive to the accuracy of diffusivity. We regard this merit of 2PT which allows for obtaining accurate thermodynamic properties using a very short MD trajectory.

5. CONCLUSION

The two-phase thermodynamic (2PT) method is extended to obtain the thermodynamic properties of fluids of linear molecules such as CO_2. In 2PT, the properties are calculated on the basis of proper statistical mechanical weighting to the normal modes, or density of state (DoS) distribution, of a fluid. The DoS can be analytically decomposed to contributions from molecular translation, rotation, and intramolecular vibrational motions. In molecular dynamic simulations, CO_2 molecules are almost never linear, and therefore, attention is required for the evaluation of the rotational DoS and the rotational weighting functions. We show that with proper treatment, both the energy (with quantum corrections) and the absolute entropy of CO_2 can be obtained from a short, 20 ps MD trajectory (when the system is equilibrated). We have examined the calculations over a wide range of conditions along the vapor−liquid coexistence curve. It is found that both the 2PT entropy and energy obtained from the FEPM2 force field are in good agreement with the experiment. The agreement in energy of vaporization between classical MD energy and experimental data is a cancellation of errors in the energy of both the vapor and the liquid phase. The 2PT energy, however, properly captures the experimental energy variations along the coexistence curve. Our results suggests that the classical force field may be refined on the basis of the 2PT properties. Finally, we also validate the 2PT entropy with those obtained from thermodynamic integration.

AUTHOR INFORMATION

Corresponding Author

*E-mail stlin@ntu.edu.tw.

ACKNOWLEDGMENT

This research was partially supported by the National Science Council of Taiwan (NSC 98-2221-E-002-087-MY3) and the Ministry of Economic Affairs of Taiwan (99-5226904000-04-04). The computation resources from the National Center for High-Performance Computing of Taiwan and the Computing and Information Networking Center of the National Taiwan University are acknowledged. W.A.G. acknowledges support from the WCU (World Class University) program through the National Research Foundation of Korea funded by the Ministry of Education, Science and Technology (R31-2008-000-10055-0). W.A.G and T.A.P. acknowledge support from DOE (DE-FE0002057.DE-AC26-07NT42677, and DE-EE0003032).

REFERENCES

(1) Penninger, J. M. L. *Supercritical fluid technology*; Elsevier Science: Amsterdam, 1985.
(2) Roberts, C. B.; Chateauneuf, J. E.; Brennecke, J. F. *J. Am. Chem. Soc.* **1992**, *114*, 8455–8463.
(3) Lee, C. T.; Ryoo, W.; Smith, P. G.; Arellano, J.; Mitchell, D. R.; Lagow, R. J.; Webber, S. E.; Johnston, K. P. *J. Am. Chem. Soc.* **2003**, *125*, 3181–3189.
(4) Schievelbein, V. H. *Method for decreasing mobility of dense carbon dioxide in subterranean formations*; Texaco Inc.: White Plains, NY, 1991.
(5) Leitner, W.; Poliakoff, M. *Green Chem.* **2008**, *10*, 730–730.
(6) Beckman, E. J. *J. Supercrit. Fluid* **2004**, *28*, 121–191.
(7) Baiker, A. *Chem. Rev.* **1999**, *99*, 453–473.
(8) Jung, J. W.; Espinoza, D. N.; Santamarina, J. C. *J. Geophys. Res., Solid Earth* **2010**, *115*, B10102.
(9) Zhou, X. T.; Fan, S. S.; Liang, D. Q.; Du, J. W. *Energy Convers. Manage.* **2008**, *49*, 2124–2129.
(10) Yezdimer, E. M.; Cummings, P. T.; Chialvo, A. A. *J. Phys. Chem. A* **2002**, *106*, 7982–7987.
(11) Merker, T.; Engin, C.; Vrabec, J.; Hasse, H. *J. Chem. Phys.* **2010**, 132.
(12) Vrabec, J.; Stoll, J.; Hasse, H. *J. Phys. Chem. B* **2001**, *105*, 12126–12133.
(13) Potoff, J. J.; Siepmann, J. I. *AIChE J.* **2001**, *47*, 1676–1682.
(14) Harris, J. G.; Yung, K. H. *J. Phys. Chem.* **1995**, *99*, 12021–12024.
(15) Zhu, A. M.; Zhang, X. B.; Liu, Q. L.; Zhang, Q. G. *Chin. J. Chem. Eng.* **2009**, *17*, 268–272.
(16) Zhang, Z. G.; Duan, Z. H. *J. Chem. Phys.* **2005**, 122.
(17) Nieto-Draghi, C.; de Bruin, T.; Perez-Pellitero, J.; Avalos, J. B.; Mackie, A. D. *J. Chem. Phys.* **2007**, *126*, 8.
(18) Galliero, G.; Nieto-Draghi, C.; Boned, C.; Avalos, J. B.; Mackie, A. D.; Baylaucq, A.; Montel, F. *Ind. Eng. Chem. Res.* **2007**, *46*, 5238–5244.
(19) Saharay, M.; Balasubramanian, S. *J. Chem. Phys.* **2004**, *120*, 9694–9702.
(20) Zhang, Y.; Yang, J. C.; Yu, Y. X. *J. Phys. Chem. B* **2005**, *109*, 13375–13382.
(21) Anderson, K. E.; Mielke, S. L.; Siepmann, J. I.; Truhlar, D. G. *J. Phys. Chem. A* **2009**, *113*, 2053–2059.
(22) Inomata, H.; Saito, S.; Debenedetti, P. G. *Fluid Phase Equilib.* **1996**, *116*, 282–288.
(23) Murthy, C. S.; Singer, K.; McDonald, I. R. *Mol. Phys.* **1981**, *44*, 135–143.
(24) Graham, C.; Pierrus, J.; Raab, R. E. *Mol. Phys.* **1989**, *67*, 939–955.
(25) Sharma, R.; Agarwal, M.; Chakravarty, C. *Mol. Phys.* **2008**, *106*, 1925–1938.
(26) Henchman, R. H. *J. Chem. Phys.* **2007**, 126.
(27) Wang, L.; Abel, R.; Friesner, R. A.; Berne, B. J. *J. Chem. Theory Comput.* **2009**, *5*, 1462–1473.
(28) Irudayam, S. J.; Plumb, R. D.; Henchman, R. H. *Faraday Discuss.* **2010**, *145*, 467–485.
(29) Shirts, M. R.; Pande, V. S. *J. Chem. Phys.* **2005**, 122.
(30) Garrido, N. M.; Jorge, M.; Queimada, A. J.; Economou, I. G.; Macedo, E. A. *Fluid Phase Equilib.* **2010**, *289*, 148–155.

(31) Scala, A.; Starr, F. W.; La Nave, E.; Sciortino, F.; Stanley, H. E. *Nature* **2000**, *406*, 166–169.
(32) Lin, S. T.; Blanco, M.; Goddard, W. A. *J. Chem. Phys.* **2003**, *119*, 11792–11805.
(33) Lin, S. T.; Maiti, P. K.; Goddard, W. A. *J. Phys. Chem. B* **2010**, *114*, 8191–8198.
(34) Pascal, T. A.; Lin, S. T.; Goddard, W. A. *Phys. Chem. Chem. Phys.* **2010**, *13*, 169–181.
(35) Lin, S. T.; Maiti, P. K.; Goddard, W. A. *J. Phys. Chem. B* **2005**, *109*, 8663–8672.
(36) Debnath, A.; Mukherjee, B.; Ayappa, K. G.; Maiti, P. K.; Lin, S. T. *J. Chem. Phys.* **2010**, 133.
(37) Kumar, H.; Mukherjee, B.; Lin, S.-T.; Dasgupta, C.; Sood, A. K.; Maiti, P. K. *J. Chem. Phys.* **2011**, *134*, 124105.
(38) Maiti, P. K.; Bagchi, B. *Nano Lett.* **2006**, *6*, 2478–2485.
(39) Nandy, B.; Maiti, P. K. *J. Phys. Chem. B* **2011**, *115*, 217–230.
(40) Vasumathi, V.; Maiti, P. K. *Macromolecules* **2010**, *43*, 8264–8274.
(41) Berens, P. H.; Mackay, D. H. J.; White, G. M.; Wilson, K. R. *J. Chem. Phys.* **1983**, *79*, 2375–2389.
(42) Carnahan, N. F.; Starling, K. E. *J. Chem. Phys.* **1970**, *53*, 600–603.
(43) Plimpton, S. *J. Comput. Phys.* **1995**, *117*, 1–19.
(44) Perry, R. H.; Green, D. W.; Maloney, J. O. *Perry's Chemical Engineers' Handbook*, 7th ed.; McGraw-Hill: New York, 1997.
(45) *NIST Chemistry WebBook*, Reference Database Number 69; National Institute of Standards and Technology: Gaithersburg, MD, 2000. http://webbook.nist.gov/chemistry/ (accessed May 2011).
(46) Hoover, W. G. *Phys. Rev. A* **1985**, *31*, 1695–1697.
(47) Hockney, R. W.; Eastwood, J. W. *Computer Simulation Using Particles*; Taylor & Francis: New York, 1989.
(48) Karasawa, N.; Goddard, W. A. *J. Phys. Chem.* **1989**, *93*, 7320–7327.
(49) Arakawa, M.; Yamamoto, J.; Kagi, H. *Chem. Lett.* **2008**, *37*, 280–281.
(50) Olijnyk, H.; Jephcoat, A. P. *Physica B* **1999**, *265*, 54–59.